Ultrafast Wiggling and Jiggling: $Ir_2(1,8\text{-diisocyanomenthane})_4^{2+}$

Martin Pižl,[a,b] Bryan M. Hunter,[c] Gregory M. Greetham,[d] Michael Towrie,[d] Stanislav Záliš,[a,]* Harry B. Gray,[c,]* Antonín Vlček[a,e,]*

[a] J. Heyrovský Institute of Physical Chemistry, Academy of Sciences of the Czech Republic, Dolejškova 3, CZ-182 23 Prague, Czech Republic
[b] Department of Inorganic Chemistry, University of Chemistry and Technology, Prague, Technická 5, CZ-166 28 Prague, Czech Republic
[c] Beckman Institute, California Institute of Technology, Pasadena, CA 91125, USA
[d] Central Laser Facility, Research Complex at Harwell, STFC, Rutherford Appleton Laboratory, Harwell Oxford, Didcot, Oxfordshire OX11 0QX, United Kingdom,
[e] Queen Mary University of London, School of Biological and Chemical Sciences, Mile End Road, London E1 4NS, United Kingdom
e-mail: zalis@jh-inst.cas.cz, hbgray@caltech.edu, a.vlcek@qmul.ac.uk

Abstract

Binuclear complexes of d^8 metals (Pt^{II}, Ir^{I}, Rh^{I},) exhibit diverse photonic behavior including dual emission from relatively long-lived singlet and triplet excited states, as well as photochemical energy-, electron-, and atom transfer. Time-resolved optical spectroscopic and X-ray studies have revealed the behavior of the dimetallic core, confirming that M-M bonding is strengthened upon $d\sigma^* \rightarrow p\sigma$ excitation. We report the bridging ligand dynamics of $Ir_2(1,8\text{-diisocyanomenthane})_4^{2+}$ (Ir(dimen)), investigated by fs-ns time-resolved IR spectroscopy (TRIR) in the region of C≡N stretching vibrations, ν(C≡N), 2000-2300 cm^{-1}. The ν(C≡N) IR band of the singlet and triplet $d\sigma^*p\sigma$ excited states is shifted by -22 and -16 cm^{-1} relative to the ground state due to delocalization of the $p\sigma$ LUMO over the bridging ligands. Ultrafast relaxation dynamics of the $^1d\sigma^*p\sigma$ state depend on the initially excited Franck-Condon molecular geometry, whereby the same relaxed singlet excited state is populated by two different pathways depending on the starting point at the excited-state potential energy surface: Exciting the long/eclipsed isomer triggers two-stage structural relaxation: 0.5 ps large-scale Ir-Ir

contraction and 5 ps Ir-Ir contraction/intramolecular rotation. Exciting the short/twisted isomer induces a ~5 ps bond shortening combined with vibrational cooling. Intersystem crossing (70 ps) follows, populating a $^3d\sigma^*p\sigma$ state that lives for hundreds on nanoseconds. During the first 2 ps, the $\nu(C{\equiv}N)$ IR bandwidth oscillates with the frequency of the $\nu(Ir-Ir)$ wave packet, ca. 80 cm^{-1}, indicating that the dephasing time of the high-frequency (16 fs)$^{-1}$ C$\equiv$N stretch responds to much slower (~400 fs)$^{-1}$ Ir-Ir coherent oscillations. We conclude that the bonding and dynamics of bridging di-isocyanide ligands are coupled to the dynamics of the metal–metal unit; and that the coherent Ir-Ir motion induced by ultrafast excitation drives vibrational dephasing processes over the entire binuclear cation.

Introduction

Investigations of the excited-state dynamics of d^8–d^8 complexes have revealed that metal-metal bonding interactions are enhanced upon electronic excitation; there is an accompanying structural response, along with energy dissipation through intramolecular vibrational modes and solvent interactions, as well as vibrational coherence and spin conversion.[1,2,3,4] Of particular interest is that the slow rates of excited singlet to triplet intersystem crossing (ISC) have allowed workers to detect and characterize the two spin states separately.[3,5,6] Many of these complexes also are redox-active, most especially as powerful reductants and oxidants in photoinduced electron- and atom transfer reactions.[1] Prototypal d^8–d^8 complexes include isocyanide-bridged di-iridium(I) and rhodium(I) complexes, as well as $[Pt_2(P_2O_5H_2)_4]^{4-}$ (Ptpop)) and its perfluoroborated counterpart $[Pt_2(P_2O_5(BF_2)_2)_4]^{4-}$.[1] Analogous

noncovalent d^8–d^8 assemblies of Rh^I, Ir^I, Pd^{II}, Pt^{II}, and Au^{III} complexes also exhibit rich photoluminescence and photochemistry.[7]

Investigations of d^8–d^8 excited-state structures and dynamics have focused on the dimetallic unit. Experiments included monitoring time-evolution of X-ray absorption, emission, or scattering by the two heavy atoms after optical excitation, or by time-resolved UV-vis spectra, whereby the behavior of $d\sigma^*p\sigma$ excited states is manifested by stimulated and spontaneous emission, as well as by excited-state absorption. For example, time-resolved X-ray absorption spectra of Pt(pop) in the EXAFS region revealed a 0.31 Å Pt–Pt bond shortening in the $^3d\sigma^*p\sigma$ state while the XANES spectrum reported on changes in electronic structure, namely depopulation of the $5d\sigma^*$ orbital.[4,8] Similarly, shortening of the Ir–Ir bond in singlet and triplet $d\sigma^*p\sigma$ states of $[Ir_2(1,8\text{-diisocyanomenthane})_4]^{2+}$ (Ir(dimen), Figure 1) was revealed by time-resolved X-ray scattering.[2,5] Femtosecond laser excitation of these complexes creates a ν(M-M) wave packet whose coherent motion is manifested by oscillations of the stimulated emission (Pt, Ir) and excited-state absorption (Pt) that persist for more than 2 ps.[3,6,9,10]
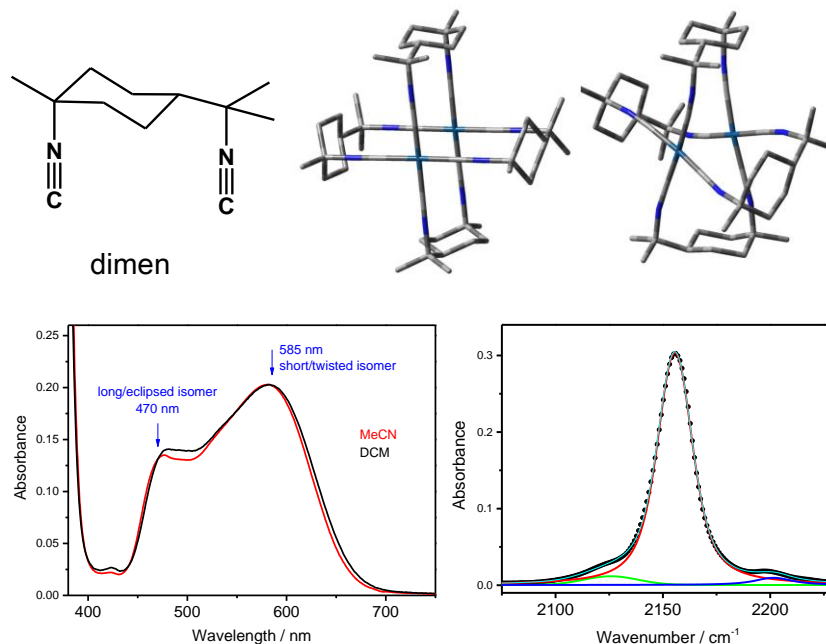
Figure 1. Top: the dimen ligand (left), calculated structures of the long/eclipsed (middle) and short/twisted Ir(dimen) isomers. Hydrogen atoms are omitted for clarity. Bottom row, left: visible absorption spectrum, the blue arrows show irradiation wavelengths used to excite selectively the two isomers. Right: FTIR ground-state spectrum in DCM (black points) decomposed into three Voigt functions (green, red, blue; sum in cyan. Parameters of the main band (red): 2156 cm^{-1}, Gaussian width 12.0 cm^{-1}, Lorentzian width 12.1 cm^{-1}, FWHM 19.7 cm^{-1}). An equivalent fit is obtained with three Lorentzian functions, only with a small discrepancy in the region of the 2202 cm^{-1} band.

In addition to X-ray and optical spectroscopic studies, excited states of isocyanide-bridged complexes are candidates for time-resolved IR (TRIR), which monitors the temporal evolution of features attributable to C≡N– stretching vibrations (ν(C≡N)). As the ν(C≡N) frequency and intensity depend strongly on both electronic and molecular structures,[11,12,13] TRIR spectroscopy undoubtedly will shed new light on d^8–d^8 photophysics, most especially on the role of ligands in excited-state dynamics.

We report TRIR spectra of Ir(dimen) measured over a broad temporal range from tens of femtoseconds to microseconds, supported by excited-state DFT calculations. Ir(dimen)

represents a challenging case, from both structural and dynamical viewpoints, as the dimen ligand has two C≡N− groups ca. 5 Å apart[14] but the metal-metal bond can be shorter, owing to ligand distortions and twisting. A delicate balance between metal-metal interactions and ligand strain gives rise to two deformational isomers (Figure 1) that coexist in solution and differ in Ir-Ir distance and C-Ir-Ir-C dihedral angle: long/eclipsed (4.3 Å, ~0°) and short/twisted (3.6 Å, ~15°).[5,14,15] Different positions of the $d\sigma^* \rightarrow p\sigma$ bands in the visible absorption spectrum made it possible to excite the long/eclipsed and short/twisted isomers separately at 470 and 585 nm, respectively, and follow the excited-state evolution by TRIR spectroscopy in the $\nu(C\equiv N)$ range as a function of the initial geometry. With Ir(dimen) as a model, we employed TRIR for the first time to monitor the response of bridging ligands to electronic excitation of a d^8-d^8 complex. We discovered a multistep relaxation cascade that depends on the excitation wavelength (that is, on the initial Franck-Condon geometry) and documented a new effect of coherent oscillations of the excited-state IR signal, thereby demonstrating that the Ir-Ir wavepacket motion affects the entire cation.

Results and Discussion

The ground-state visible absorption spectrum of Ir(dimen) (Figure 1) exhibits peaks at ca. 480 and 590 nm attributable[9,12,14,15] to the long/eclipsed and short/twisted isomers, respectively. Solution IR spectra of the two isomers are indistinguishable,[12] with a strong band at ~2160 cm^{-1} (assigned to two quasidegenerate antisymmetrical C≡N stretching vibrations ($\nu(C\equiv N)$)) and two very weak $\nu(C\equiv N)$ features at 2126 and 2202 cm^{-1} (Figure 1). Optical excitation of either isomer results in instantaneous appearance of a down-shifted positive

transient band at ~2136 cm^{-1} and a partly overlapping negative bleach band at ~2160 cm^{-1}, attributable to the ^{1}dσ*pσ excited state and depleted ground-state population, respectively (Figure 2 – top, green spectra). The IR signal undergoes rich dynamic evolution that is excitation-wavelength dependent at early times after excitation (0 – ca. 15 ps) but converges to the same behavior on a longer timescale. Finally, the TRIR signal vanishes with hundreds-of-nanoseconds single-exponential kinetics.

Excited-state dynamics after 470 and 585 nm laser-pulse excitation were analyzed by multiexponential global fitting of TRIR spectra, assuming a sequential mechanism. (This kind of analysis produces "population lifetimes". Periodic oscillations that might be superimposed on the kinetic traces are averaged out.) The TRIR temporal evolution is described by 3-4 exponential lifetimes and the corresponding decay associated (DA) spectra (Figure 2). Band positions and kinetics parameters are summarized in Tables 1 and 2, respectively. All observed ν(C≡N) IR bands of the ground- and excited Ir(dimen) have predominantly Lorentzian shapes (Figures 1, S1).
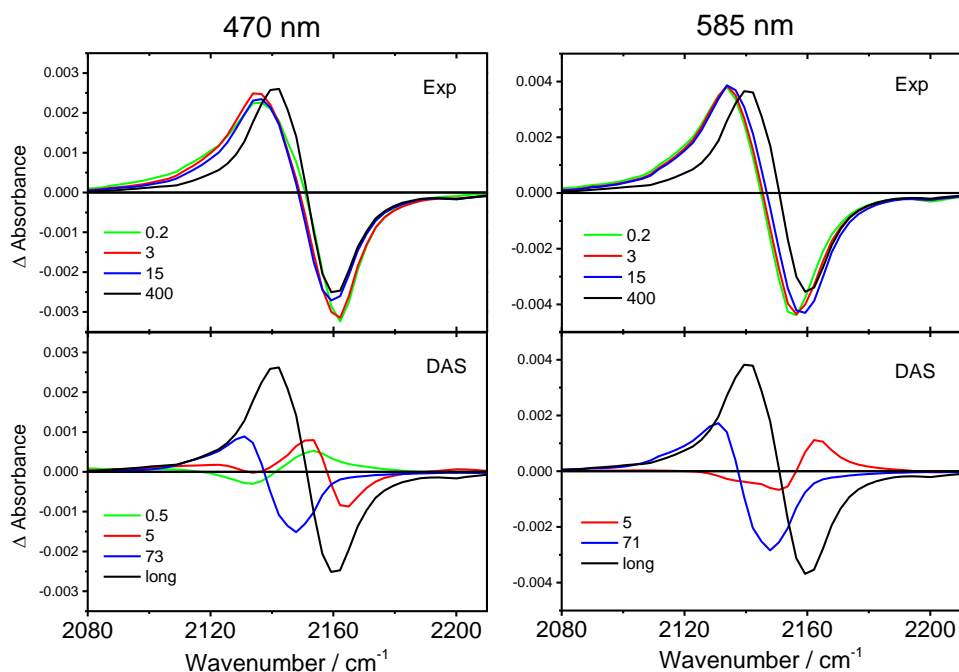
Figure 2. Time-evolution of difference IR spectra of Ir(dimen) in MeCN after 470 nm (left) and 585 nm (right) excitation measured with a magic angle orientation between Vis pump and IR probe polarizations. Top: difference TRIR spectra measured at selected time delays. Bottom: decay associated spectra obtained by multiexponential global fitting. The "long" component corresponds to the final nanosecond decay and bleach recovery. Negative and positive DA spectra denote a rise and decrease of the IR signal with time, respectively. (See Figure S2 for details of the 2130-2160 cm^{-1} region and Figures S3-S4 for spectra in DCM and THF.)

Exciting the long/eclipsed isomer at 470 nm.

The broad IR feature that emerges immediately upon excitation consists of a positive transient band at ~2135 cm^{-1} that partly overlaps a bleach at ~2162 cm^{-1}. Another very weak bleached ground-state band occurs at 2203 cm^{-1} (green spectrum in Figure 2, top-left). Initially, the most pronounced changes occur in the region between the transient band maximum and bleach minimum. The ~2135 cm^{-1} transient feature undergoes a ~2 cm^{-1} downshift occurring with a 0.5 ps lifetime, as is demonstrated by the derivative-like shape of the 0.5 ps DA spectrum that shows a maximum (signal decay) at 2154 cm^{-1} and a negative minimum around 2136 cm^{-1}

(signal rise). Independently, the 0.5 ps downshift of the transient band is documented in plots of the transient-band maximum wavenumber (obtained by Lorentzian fitting) vs. time (Figure 3). The initial band shift also is seen when comparing 0.5 and 5 ps evolution association (EA) spectra (Figure S6) that approximately correspond to difference IR spectra at the moment of excitation and at the end of the 0.5 ps process, respectively. The DA spectra of the second kinetics step (5 ps) indicate a combined narrowing and small continuing downshift. The 0.5 and 5 ps DA spectra differ in the bleach region above 2160 cm^{-1}, where the 5 ps kinetics involve a weak rising signal (appearing as partial bleach recovery). This behavior is due to an emergence of a weak transient feature corresponding to the downshifted 2202 cm^{-1} ground-state vibration. (This assignment is supported by DFT excited-state vibrational analysis, Tables S1, S2.) The 5 ps DA spectrum is slightly positive in the 2200 cm^{-1} region, indicating bleach deepening, probably due to a diminishing broad transient absorption signal in the same region. (The deepening of the 2200 cm^{-1} bleach band essentially excludes the possibility of a partial 5 ps ground-state recovery.) The similar shapes of the 0.5 and 5 ps DA spectra indicate a similar nature of the underlying processes. In accordance with the results of previous QM/MM simulations,[2,16] we assign the 0.5 and 5 ps dynamics to biphasic Ir-Ir compression that is coupled with ligand twisting and, presumably, with solvation changes[16] in the second (5 ps) step.

The DA spectrum of the third kinetics component (~70 ps) is typical of conversion between two transient species, showing decay of the 2136 cm^{-1} feature and concomitant rise of a new band at 2142 cm^{-1} that tails to ≥2180 cm^{-1}. The bleach bands stay constant, excluding concomitant ground-state recovery. This process was attributed to intersystem crossing (ISC)

from the $^1d\sigma^*p\sigma$ state to the corresponding triplet that also has been detected[5] on a ~100 ps timescale by X-ray scattering. The ~70 ps lifetime is close to that of stimulated fluorescence decay (~65 ps).[5] Both the 2142 cm^{-1} transient feature (due to $^3d\sigma^*p\sigma$ state) and the bleach then undergo slow decay on a hundreds-of-nanoseconds timescale, longer than the time-range of the ultrafast experiments. (Independent ns TRIR measurements estimated the corresponding lifetime as ca. 170 ns (MeCN), 400 ns (DCM), or 350 ns (THF), accelerated by traces of oxygen. The slow decay and oxygen-quenching further support an assignment of the 2142 cm^{-1} feature to the triplet state.) Having established the ~70 ps process as ISC, we identified the ~70 ps and "long" EA spectra (Figure S6) with difference IR spectra of the relaxed singlet and triplet $d\sigma^*p\sigma$ excited states, respectively, and determined the corresponding peak wavenumbers (Table 1) by their Lorentzian fits (Figure S7).
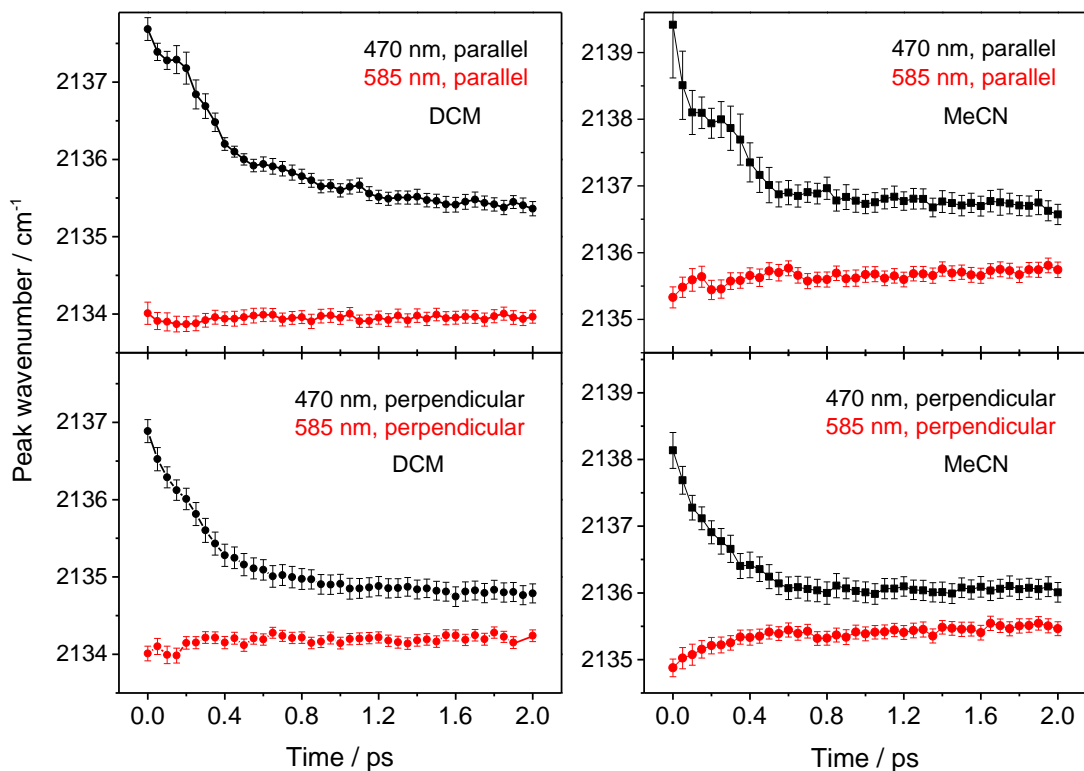
Figure 3. Time dependence of the maximum wavenumber of the transient IR band of Ir(dimen) in DCM and MeCN after 470 and 585 nm excitation. (Data in MeCN/magic angle are shown in Figure S5).

Table 1. Peak maxima (cm^{-1}) of Ir(dimen) ν(C≡N) IR bands in its electronic ground state as well as singlet and triplet dσ*pσ excited states. Determined by two-Lorentzian fits of the evolution associated spectra corresponding to the ISC and "long" kinetics components, respectively. (For weak GS bands, see Tables S1-S2.)

	GS	Singlet	Triplet	Δ(S-GS)	Δ(T-GS)	Δ(S-T)
MeCN	2158	2136	2142	-22	-16	-6
DCM	2157	2134	2141	-23	-16	-7
THF	2157	2134	2140	-23	-17	-6

Table 2. Time constants determined by multiexponential global fitting of Ir(dimen) TRIR spectra under various experimental conditions (solvent / excitation wavelength / polarization).

Conditions	ultrafast	ps	ISC
MeCN / 470 nm / magic	0.46±0.05	4.9±0.1	73±3
MeCN / 585 nm / magic	-	4.9±0.1	72±1
MeCN / 470 nm / parallel	0.95±0.03	7.0±0.2	68±1
MeCN / 585 nm / parallel	-	7.9±0.1	79±1
MeCN / 470 nm / perp	0.29±0.01	4.7±0.1	70±1
MeCN / 585 nm / perp	-	4.5±0.1	68±1
DCM / 470 nm / magic	0.56±0.02	6.6±0.1	108±1
DCM / 585 nm / magic	-	6.4±0.1	110±1
DCM / 470 nm / parallel	1.00±0.03	8.2±0.3	111±2
DCM / 585 nm / parallel	-	10.7±0.7	120±3
DCM / 470 nm / perp	0.51±0.02	7.2±0.2	100±1
DCM / 585 nm / perp	-	5.8±0.6	104±5
THF / 470 nm / magic	0.56±0.02	7.6±0.2	102±2
THF / 585 nm / magic	-	8.2±0.1	105±1

Exciting the short/twisted isomer at 585 nm.

Comparing the right and left columns of Figure 2 (compare also the 5 and 70 ps EA spectra in Figure S6) reveals that TRIR spectral evolution is different than that after 470 nm

excitation. The 0.5 ps kinetics component is missing after 585 nm excitation and, accordingly, the spectra measured at 0.2 and 3 ps are nearly identical. The first kinetics step occurs with a ~5 ps lifetime and the corresponding DA spectrum suggests a small shift of the main transient band to higher wavenumbers that also is indicated by the small gradual shift of its maximum wavenumber (Figure 3). This behavior is characteristic of vibrational cooling and solvent restructuring.[17,18] At longer time delays (>20 ps), the TRIR spectral evolution is virtually identical to that observed after 470 nm excitation: a ~70 ps conversion of the $^1d\sigma^*p\sigma$ band at 2136 cm^{-1} to a $^3d\sigma^*p\sigma$ feature that lies 6 cm^{-1} higher. Slow (hundreds of ns) decay of both the transient and the bleach follows.

Solvent and polarization effects

Changing the solvent from MeCN to DCM or THF changes neither the spectra nor dynamic evolution but slightly prolongs all the lifetimes (Table 2). Peak wavenumbers and their shifts upon excitation are virtually solvent independent (Table 1, Figure S6). The upshift of the transient band accompanying the ~5 ps kinetics after 585 nm excitation is more pronounced in MeCN and THF than in DCM.

TRIR spectra measured with a perpendicular orientation of visible-pump and IR-probe polarizations are more intense than those obtained at a parallel orientation (Figures S8, S9). This is accordance with the perpendicular orientation of the transition moments of the $d\sigma^* \rightarrow p\sigma$ electronic transition (z) and of the most IR-intense $\nu(C\equiv N)$ vibrations. Anisotropy is approximately constant across the transient band. It is independent of time after 585 nm excitation (ca. -0.13 and -0.17 in MeCN and DCM, resp.), while a small decrease occurred in 1-2

ps after exciting at 470 nm (from ca. -0.10 at 0.2 ps in MeCN). Intensity-normalized spectra are very similar at both polarizations with the exception of the ~2200 cm^{-1} bleach in 585 nm – excited spectra that is stronger under parallel polarization since it belongs to a z-polarized B_1 vibration (Table S1). Moreover, parallel-polarized spectra measured at early times after 470 nm excitation in the steep region between the transient and the bleach are broadened and/or upshifted by 2-3 cm^{-1} relative to the perpendicular spectra. This broadening could arise from the contribution of an excited-state B_1 vibration, predicted by DFT (Table S1). The lifetimes of the ~0.5 ps (at 470 nm excitation) and ~5 ps (both 470 and 585 nm excitation) steps are comparable at magic-angle and perpendicular polarizations but 1.5-2 times longer at parallel polarization (Table 2). It is possible that the perpendicular- and parallel- polarized $\nu(C\equiv N)$ vibrations within the transient IR band respond differently to different relaxation motions.

At either excitation wavelength, the 70-120 ps (ISC) DA spectra in the bleach region (around 2160 cm^{-1}) are positive in parallel and negative in perpendicular polarizations; and the corresponding lifetime in DCM is polarization-dependent (Table 2). This behavior is attributable to molecular rotation occurring on a timescale comparable with ISC (~100 ps), which is not related to the excited-state dynamics.

Coherent oscillations of IR transient signals

Several damped, approximately sinusoidal, oscillations are superimposed during the first two picoseconds on kinetic traces measured at the red side of the ~2135 cm^{-1} transient band of the $^1d\sigma^*p\sigma$ excited state and above the ~2160 cm^{-1} bleach (Figures 4, 5, and S10-12). They occur with a period of 390-430 fs (i.e., 86-76 cm^{-1}) attributable to Ir-Ir stretching in the $^1d\sigma^*p\sigma$

excited state. (75-80 cm^{-1} ν(Ir-Ir) was determined[9] independently from oscillating stimulated emission while QM/MM calculations revealed an additional involvement of delocalized deformational motions.[16]) Oscillations vanish in the region of the transient band maximum and bleach minimum. In the steep region between the transient and bleach, they are observable only in 470 nm – excited, parallel-polarized spectra (where the transient band is slightly broadened/shifted to higher wavenumbers). Because of the broad wings of the Lorentzian bands, oscillations are weakly apparent even at wavenumbers far away from the transient maximum. In the region above the bleach (usually >2180 cm^{-1}), they are attributable either to an oscillating high-wavenumber tail of the ~2135 cm^{-1} feature or to another weak transient (calculated at 2185 cm^{-1}, Table S1). The latter explanation is supported by the phase shift between oscillations in low- and high regions of the spectrum. Oscillations disappear at the edges of the investigated spectral range where the background beat at slightly negative times is the strongest. Hence, they cannot originate from follow-up background fluctuations. (Great care was taken to exclude experimental artifacts, Figure S13.) 2-3 oscillations were observed under all experimental conditions (solvent, excitation wavelength, polarization) but they were most intense after 585 nm excitation when up to 5 oscillations were observed over the first 2 ps. The oscillatory character of the kinetics traces was further confirmed by Fourier transformation (FFT, Figures S14-15) that produced a single strong peak at 77-88 cm^{-1}. FFT of traces measured close above the bleach minimum show peaks at ca. 22 and 44-55 cm^{-1} that could belong to the ground-state Ir-Ir stretch, known[9] to occur at 11 (long/eclipsed) and 48 (short/twisted) cm^{-1}. The 77-88 cm^{-1} FT peak merges with the noise in regions of the transient band maximum and bleach minimum, as well as below ~2020 and above ~2230 cm^{-1}.
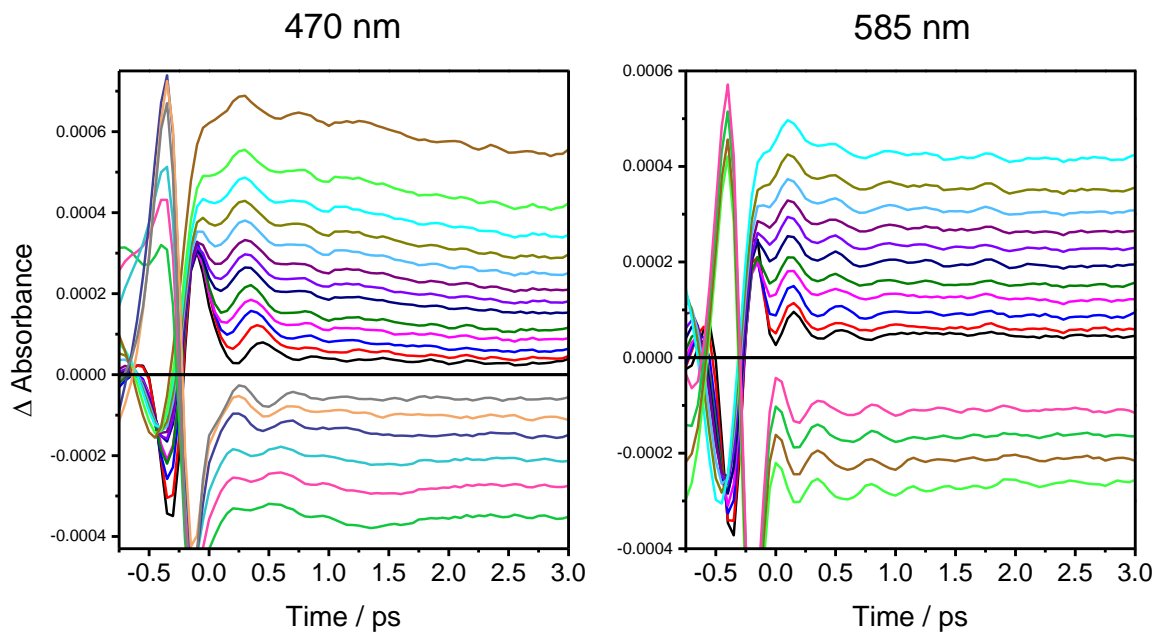
Figure 4. Selected kinetics traces measured after 470 and 585 nm excitation of Ir(dimen) in MeCN with magic angle between pump and probe beam polarizations. 3-point averaging applied. Traces in the left panel were measured at (from top down): 2112, 2109, 2106, 2103, 2101, 2098, 2095, 2093, 2087, 2085, 2079, 2071, 2058 cm^{-1}, break line, 2218, 2206, 2200, 2188, 2185, 2182 cm^{-1}. Note the long-period low-amplitude sinusoidal modulations on the last three traces, attributable to the ground-state ν(Ir-Ir) wavepacket. Right panel: 2101, 2098, 2095, 2093, 2090, 2087, 2085, 2082, 2077, 2069, 2058 cm^{-1}, break line, 2215, 2209, 2206, 2203 cm^{-1}. Raw data obtained with different polarizations in DCM and THF are shown in Figures S10-12.
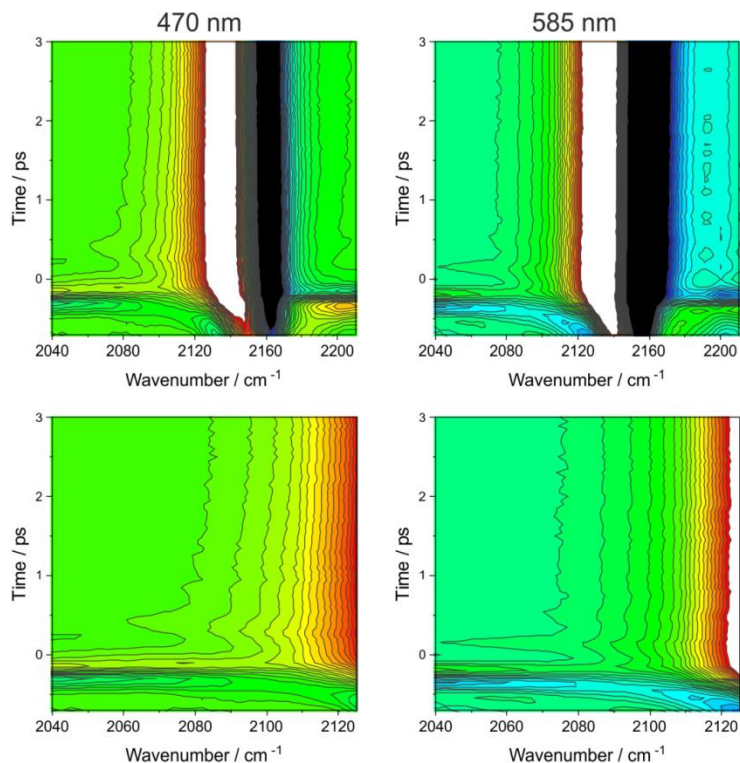
Figure 5. Time-wavenumber maps of Ir(dimen) TRIR spectra in MeCN (excitation at 470 and 585 nm). Top: full spectral range, bottom: detail of the low-wavenumber side of the excited-state band. Black-blue and green-red-white colors indicate negative and positive ΔA values, respectively. Constructed from raw data (no smoothing).

2D TRIR maps (Figure 5) show oscillations manifested as streaks along the wavenumber axis, indicating periodic band broadening and narrowing. This behavior was confirmed by fitting TRIR spectra measured every 50 fs over the 0-2000 fs interval to two or three Lorentzians (Figure S7) describing the transient excited-state band and one (~2157 cm^{-1}) or two (~2157, ~2202 cm^{-1}) bleach bands. Plotting the bandwidth as a function of time (Figure 6) revealed that intensity oscillations of kinetics traces are actually caused by bandwidth oscillations. They are most prominent at magic-angle and parallel polarizations but weak in 585 nm/perpendicularly polarized spectra. (Similar oscillations, albeit with worse S/N ratio, are exhibited by integrated

band areas.) In contrast with bandwidths, the peak maximum wavenumber does not show any periodicity (Figure 3).
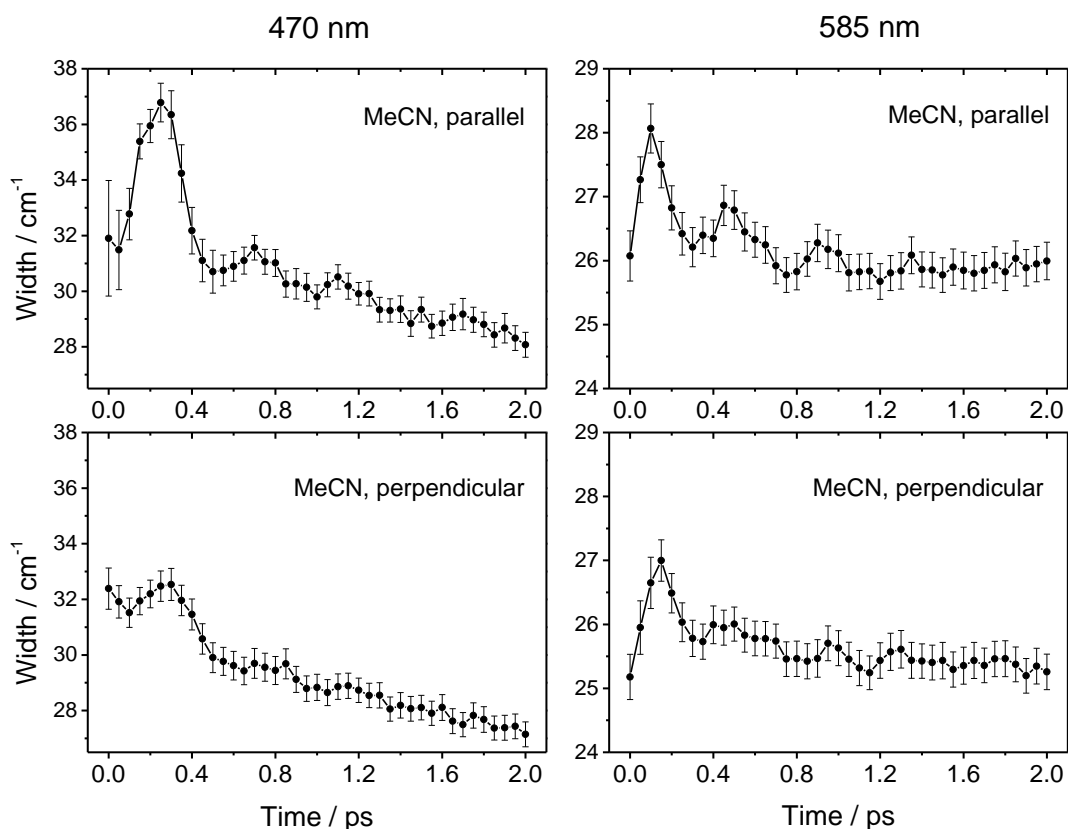

Figure 6. Time dependence of the width (FWHM) of the transient IR band of Ir(dimen) in MeCN after 470 and 585 nm excitation. (Results in MeCN-magic angle and DCM are shown in Figures S16 and S17, respectively.)

*Characterization of excited states and their vibrations*

TDDFT calculations indicate that the lowest electronic transition of each deformational isomer is 95-99% HOMO→LUMO (i.e., dσ*→pσ).[12] Whereas the HOMO is ~90% Ir in character, the LUMO is strongly mixed (ca. 35% Ir, 60% π*(C≡N) at the ground-state geometry;[12] and 29% Ir, 63% C≡N at the optimized ^{1}dσ*pσ geometry, Tables S3-S5). The substantial π*(C≡N) participation in the LUMO introduces MMLCT (metal-metal to ligand charge transfer) character

16

in both dσ*pσ excited singlet and triplet states, with the result that the isocyanide ligand will be very sensitive to changes in Ir–Ir bonding. TDDFT optimization of excited-state structures (in MeCN - continuum dielectric model, Table S6) yielded a single stable minimum for ^{1}dσ*pσ (Ir-Ir: ~2.88 Å, 42° twist), and also one for ^{3}dσ*pσ (~2.85 Å, 42°). These Ir-Ir distances are very near the experimental values[2,5] of 2.92 and 2.90 Å, respectively (determined in MeCN by X-ray scattering), and substantially shorter than those in either the long/eclipsed (4.3 Å)[5] or short/twisted (3.6 Å)[5] ground-state isomer. The slightly longer distance in the excited singlet than triplet is typical for d^8–d^8 complexes.[1] A second minimum 0.1 eV higher in energy corresponding to an eclipsed triplet state (2.94 Å, ~0°) was found by the UKS procedure (but not by TDDFT), suggesting that the ^{3}dσ*pσ structure is not rigid. (Excited-state structures are shown in Figure S18.) The spin density in the optimized ^{3}dσ*pσ state (Figure S19) is largely localized in π*(C≡N) orbitals oriented parallel with the Ir–Ir axis. Overall, the excited-state structures and triplet spin-density distribution are similar to those in the 1-electron reduced species, Ir(dimen)$^+$.[12] The ground-state ~2157 cm^{-1} band was assigned by DFT to quasidegenerate B_2 (y-polarized) and B_3 (x-polarized) ν(C≡N) vibrations, while the 2202 cm^{-1} band belongs to a z-polarized B_1 mode (D_2 group).[12] The corresponding vibrational motions are very similar to those calculated for the ground state.[12] DFT calculations qualitatively reproduce the downshift of B_2 and B_3 ν(C≡N) frequencies upon excitation but do not account for the different ν(C≡N) values in the triplet and singlet excited states (Tables S1, S2). (A very smaller shift of -6 cm^{-1} was calculated for the twisted form of the triplet, indicating that it does not contribute to TRIR spectra.)

Electronically excited Ir(dimen) and its dynamics

Electronic excitation preserves the degeneracy of the B_2 and B_3 $\nu(C\equiv N)$ modes, confirming (in accord with DFT) that the ground state and the singlet- and triplet dσ*pσ excited states have very similar molecular geometries. The $\nu(C\equiv N)$ IR features of relaxed singlet and triplet dσ*pσ excited states are shifted by -22 and -16 cm^{-1} relative to the ground state. The 6 cm^{-1} $\nu(C\equiv N)$ difference, as well as the Ir–Ir distance ~0.02 Å longer in the triplet,[2,5] show that the bonding in singlet and triplet dσ*pσ states is similar but not identical (as often assumed). The Lorentzian excited-state $\nu(C\equiv N)$ band shape (also found for [3]MLCT states of W(C$\equiv$N–Aryl)$_6$ complexes[11]) is due mainly to homogeneous line broadening that in turn indicates uniformity in the interactions between the C$\equiv$N oscillator and solvent molecules over the ensemble of excited molecules.

According to DFT, the downshift of the $\nu(C\equiv N)$ band upon excitation results from Ir$\rightarrow\pi$*(C$\equiv$N) charge transfer in the singlet and triplet dσ*pσ excited states owing to ~60% π*(C$\equiv$N) participation in the pσ LUMO. Ir-Ir shortening (by 33 and 10% relative to long/eclipsed and short/twisted ground-states) is the main structural effect of excitation, caused by dσ* depopulation and pσ population (for comparison, 1-electron occupancy of the pσ orbital upon reduction causes 29 and 5% shortening, respectively (DFT)[12]). The charge transfer component is delocalized over the eight ligating C$\equiv$N- groups, resulting only in ~0.005 Å Ir-C lengthening and virtually no effect on C$\equiv$N distances (Tables S6-7).
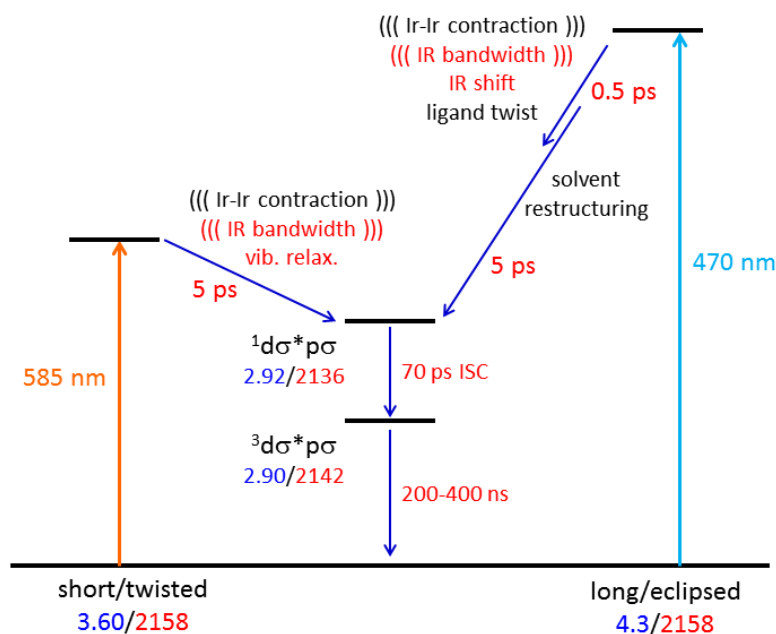
Scheme 1. Excited-state dynamics of Ir(dimen). Upon 585-nm excitation, the short/twisted isomer (left) undergoes ca. 0.7 Å Ir-Ir contraction in 5 ps to produce a relaxed $^1d\sigma^*p\sigma$ excited state; and following 470-nm excitation, the long/eclipsed isomer undergoes biphasic (0.5, 5 ps) 1.4 Å Ir-Ir contraction that at later stages is coupled with ligand twisting and restructuring of the first solvation sphere.[2,5,9,16] Interestingly, ~70 ps ISC occurs after excitation of each isomer. Ir-Ir distances[2,5] (Å) determined by time-resolved X-ray scattering are shown in blue. Results from this work are shown in red, $\nu(C{\equiv}N)$ values in cm^{-1}. ((( ))) denotes coherent oscillations.

Excitation-wavelength dependent dynamics of the $^1d\sigma^*p\sigma$ state reflect different pathways leading from the long/eclipsed and short/twisted Franck-Condon points on the excited-state potential energy surface to the common short/twisted relaxed geometry. Scheme 1 summarizes the relaxation steps involved and their effects on the Ir-Ir distance as well as on the $\nu(C{\equiv}N)$ IR band. Excitation of the long-eclipsed isomer (470 nm) is followed by 0.5 ps large-amplitude Ir-Ir contraction that is completed in a ~5 ps step that also includes ligand twisting[16] and restructuring of the solvent shell.[2] A 2 cm^{-1} downshift of the $\nu(C{\equiv}N)$ band during the first 1 ps is attributable to electron-density redistribution (increasing π back donation) in the course of initial Ir-Ir contraction. Neither of these steps is accompanied by vibrational cooling, as it would

appear that most of the excess energy is used in overcoming nuclear reorganization barriers required for structural rearrangements. Only the second phase of Ir-Ir shortening, but no ligand twisting, is required after exciting the short/twisted isomer at 585 nm. Hence, the 0.5 ps step is missing and $^1d\sigma^*p\sigma$ relaxation consists only of the 5 ps low-amplitude contraction, together with cooling and, presumably, solvent relaxation. (Solvent involvement in the excited-state dynamics of both isomers is indicated by a small increase of all relaxation lifetimes on going from MeCN to DCM and THF, where solvation is less pronounced. Moreover, DFT-optimized structures of Ir(dimen) solvated with four MeCN molecules suggest mostly random MeCN arrangement in the ground state, whereas the $^3d\sigma^*p\sigma$ state shows some preference for an Ir⋯N(MeCN) orientation (Figure S20).)

Both 470 and 585 nm excitations create a ν(Ir-Ir) wave packet (75-80 cm^{-1}) that modulates $^1d\sigma^*p\sigma$ stimulated emission during the first ~2 ps.[9] Of interest is that the width of the $^1d\sigma^*p\sigma$ ν(C≡N) IR band oscillates with approximately the same frequency. Since the ν(C≡N) vibrational period is much shorter (16 fs) than that of the ν(Ir-Ir) wave packet (445-417 fs), high-frequency C≡N stretching vibrations are affected by the "instantaneous" position of the ν(Ir-Ir) wave packet – that is, by the "instantaneous" Ir-Ir distance. The two motions could be coupled anharmonically or electronically (i.e., through electron density redistribution between pσ and π^*(C≡N−) orbitals in the course of wave packet motion). However, these mechanisms would result in an oscillating ν(C≡N) band position that was not observed. Instead, the excited-state ν(C≡N) band responds to coherent Ir-Ir motion by changing its width, indicating that Ir-Ir wave packet motion affects primarily the ν(C≡N) dephasing time T_2. (Homogeneous IR bandwidth Γ (in cm^{-1}) = $1/\pi c T_2$; and $1/T_2 = 1/2T_1 + 1/T_2^* + \Gamma_{or}$, where c is the speed of light, T_1 is the

population lifetime of the v=1 $\nu(C\equiv N)$ level, T_2^* is the pure dephasing time, and Γ_{or} is a contribution from orientational effects.)[19,20,21,22,23] The homogeneous (Lorentzian) excited-state IR band shape and its large width essentially exclude the possibility that pure dephasing is the predominant broadening mechanism, since unrealistically large (>100 cm^{-1}) fast frequency fluctuations would be required. Hence, we found it necessary to consider all three contributing terms, T_1, T_2^*, and Γ_{or}. The Ir-Ir oscillations are accompanied by changes in the twist angle, the $C\equiv N-$ angle, and movement of Ir atoms in and out of IrC$_4$ planes.[12,16] These structural changes modulate anharmonic coupling between $\nu(C\equiv N)$ and low-frequency intramolecular modes, as well as interaction with the solvent by changing the exposure of Ir and N atoms.[16] Anharmonic coupling and solvent interactions determine both the population- and pure dephasing times; and coherent Ir-Ir motion would affect them in concert, resulting in simultaneous bandwidth oscillations. (For example, changing T_1 between 5 and 1 ps depending on the initial position of the ν(Ir-Ir) wave packet would account for the observed effect.) The orientational term Γ_{or} could play an important role because of the presence of two quasidegenerate B$_2$(y) and B$_3$(x) vibrations in the main $\nu(C\equiv N)$ spectral feature, which merge into a degenerate E(x,y) mode in the D$_4$ twisted Ir$_2$C$_8$ core. Rotation of the vibrational transition dipole moment through corresponding x,y vibrational motions occurs independently of the molecular rotation on a timescale of units of picoseconds (or faster). (This type of rotational dephasing was studied in detail for the T$_{1u}$ $\nu(C\equiv O)$ mode of W(CO)$_6$.[23,24]) In the case of Ir(dimen), internal rotational dephasing will be modulated by Ir-Ir oscillations through changes in the twist angle. Whatever the detailed mechanism is, it suggests that dephasing of the high-frequency bridging-ligand vibration retains a "memory" of the initial Ir-Ir wavepacket position. To our knowledge, we are

reporting the first observation of a high-frequency vibration responding to the slower coherent motion of a low-frequency wave packet.

Whereas ultrafast $^1d\sigma^*p\sigma$ relaxation depends on the initially excited deformational isomer, TRIR spectra after ~20 ps as well as the ISC kinetics are excitation-wavelength independent, indicating that both short/twisted and long/eclipsed isomers converge to the same relaxed $^1d\sigma^*p\sigma$ excited-state structure in a few tens of picoseconds after excitation. ISC from the relaxed $d\sigma^*p\sigma$ singlet excited state to the corresponding triplet is symmetry-forbidden. In d^8–d^8 complexes, ISC requires either a structural distortion to promote spin-orbit coupling (SOC) between the $d\sigma^*p\sigma$ singlet and triplet or a low-lying intermediate state allowing second-order SOC and/or a thermally activated pathway.[1,3,25,26,27,28] The ~70 ps ISC in Ir(dimen) is faster than in the structurally more rigid isocyanide-bridged complexes of Rh(I) and Ir(I) (230 ps – 1.3 ns).[1,29,30] The dimen ligand flexibility likely enables ISC-promoting structural distortions through thermal fluctuations.

We conclude that TRIR spectroscopy can provide detailed insights into the structural and dynamical properties of electronically excited d^8–d^8 complexes. We have found that the bridging ligands in Ir(dimen) respond to structural and electronic changes caused by $d\sigma^*{\rightarrow}p\sigma$ excitation; and that this response depends on the initial Franck-Condon geometry. Moreover, the ligand C≡N bonds (vibrations) respond to Ir-Ir wave packet motion, as well as to the singlet/triplet spin change. The combination of TRIR spectroscopic with optical[9] and X-ray scattering data (that report on the dimetallic unit)[2,5] along with DFT as well as QM/MM simulations[2,16] sheds new light on Ir(dimen) excited-state behavior (Scheme 1). As the complex cation is a promising electrocatalyst for CO_2 reduction,[31] its photochemical (potentially

photocatalytic) reactivity needs to be explored in more depth. Looking ahead, TRIR has the potential to monitor interactions between electronically excited Ir(dimen) and substrates, including accompanying changes in electron density distributions and Ir oxidation states. Our finding of bridging-ligand vibrational response to Ir-Ir wave packet oscillations demonstrates that coherent effects in d^8–d^8 complexes[1,3,6,9] extend well beyond the central dimetallic unit, thereby indicating that excited-state reactions (e.g., electron-, energy-, or atom transfer) could be coupled to intramolecular coherent motions triggered by ultrafast excitation.

Experimental section

Sample preparation. The BARF ({3,5-$(CF_3)_2C_6H_3$}$_4$B) salt of Ir(dimen) was synthesized and characterized according to literature methods.[14] Solutions were made in anhydrous solvents (Sigma-Aldrich SureSeal) and handled under nitrogen. CaF_2 spectroscopic cells were scanned-rastered in two dimensions during measurements.

TRIR spectroscopy. Measurements were performed using the LIFEtime instrument[32] at the STFC Rutherford Appleton Laboratory (Lasers for Science facility), UK. 470 and 585 nm, ~200 fs fwhm, 250 nJ pulses were used as a pump, ~180 fs mid-IR pulses were used as a probe. Polarization was controlled by a half-wavelength plate in the pump-beam path. Experimental points are separated by ~2.5 cm^{-1}.

Quantum chemical calculations. Structures and vibrations of the singlet- and triplet excited states were obtained by TDDFT. Triplet state was also calculated using the UKS approach. All calculations presented above were performed on the *trans* 2:2 orientational isomer of

Ir(dimen) in PCM-modelled MeCN. Further computational details and discussion of the

orientational isomerism are provided in the SI.

■ ASSOCIATED CONTENT

Supporting Information

The Supporting Information is available free of charge on the ACS Publications website at DOI:
Shape fits of TRIR spectra, TRIR and corresponding decay-associated spectra in MeCN, DCM, and THF at magic, parallel, and perpendicular polarizations and details of the 2030-2060 cm^{-1} region, time dependences of the transient peak position and width and TRIR kinetics traces obtained at various experimental conditions together with their Fourier transforms, calculated excited-state structures and spin-density distribution, experimental and calculated ν(C≡N) wavenumbers, MO energies and compositions, computational details, and a comment on orientational isomerism.

■ AUTHOR INFORMATION

Corresponding Authors

*E-mail for S.Z.: stanislav.zalis@jh-inst.cas.cz

*E-mail for H.B.G.: hbgray@caltech.edu

*E-mail for A.V.: a.vlcek@qmul.ac.uk

Notes

The authors declare no competing financial interest.

References

1. Gray, H. B.; Záliš, S.; Vlček, A., Electronic structures and photophysics of d^8-d^8 complexes *Coord. Chem. Rev.* **2017,** *345*, 297-317.
2. van Driel, T. B.; Kjær, K. S.; Hartsock, R. W.; Dohn, A. O.; Harlang, T.; Chollet, M.; Christensen, M.; Gawelda, W.; Henriksen, N. E.; Kim, J. G.; Haldrup, K.; Kim, K. H.; Ihee, H.; Kim, J.; Lemke, H.; Sun, Z.; Sundström, V.; Zhang, W.; Zhu, D.; Møller, K. B.; Nielsen, M. M.; Gaffney, K. J., Atomistic characterization of the active-site solvation dynamics of a model photocatalyst. *Nat. Comm.* **2016,** *7*, 13678.
3. van der Veen, R. M.; Cannizzo, A.; van Mourik, F.; Vlček, A., Jr. ; Chergui, M., Vibrational Relaxation and Intersystem Crossing of Binuclear Metal Complexes in Solution. *J. Am. Chem. Soc.* **2011,** *133*, 305-315.

4. van der Veen, R. M.; Milne, C. J.; El Nahhas, A.; Lima, F. A.; Pham, V.-T.; Best, J.; Weinstein, J. A.; Borca, C. N.; Abela, R.; Bressler, C.; Chergui, M., Structural Determination of a Photochemically Active Diplatinum Molecule by Time-Resolved EXAFS Spectroscopy. *Angew. Chem. Int. Ed.* **2009,** *48*, 2711 − 2714.

5. Haldrup, K.; Harlang, T.; Christensen, M.; Dohn, A.; van Driel, T. B.; Kjær, K. S.; Harrit, N.; Vibenholt, J.; Guerin, L.; Wulff, M.; Nielsen, M. M., Bond Shortening (1.4 A) in the Singlet and Triplet Excited States of $[Ir_2(dimen)_4]^{2+}$ in Solution Determined by Time-Resolved X-ray Scattering. *Inorg. Chem.* **2011,** *50*, 9329–9336.

6. Monni, R.; Auböck, G.; Kinschel, D.; Aziz-Lange, K. M.; Gray, H. B.; Vlček, A.; Chergui, M., Conservation of vibrational coherence in ultrafast electronic relaxation: The case of diplatinum complexes in solution. *Chem. Phys. Lett.* **2017,** *683*, 112-120.

7. Yam, V. W.-W.; Au, V. K.-M.; Leung, S. Y.-L., Light-Emitting Self-Assembled Materials Based on d^8 and d^{10} Transition Metal Complexes. *Chem. Rev.* **2015** *115*, 7589−7728.

8. van der Veen, R. M.; Kas, J. J.; Milne, C. J.; Pham, V.-T.; El Nahhas, A.; Lima, F. A.; Vithanage, D. A.; Rehr, J. J.; Abela, R.; Chergui, M., L-edge XANES analysis of photoexcited metal complexes in solution. *Phys. Chem. Chem. Phys.* **2010,** *12*, 5551–5561.

9. Hartsock, R. W.; Zhang, W.; Hill, M. G.; Sabat, B.; Gaffney, K. J., Characterizing the Deformational Isomers of Bimetallic $Ir_2(dimen)_4^{2+}$ (dimen = 1,8-diisocyano-p-menthane) with Vibrational Wavepacket Dynamics. *J. Phys. Chem. A* **2011,** *115*, 2920–2926.

10. Cho, S.; Mara, M. W.; Wang, X.; Lockard, J. V.; Rachford, A. A.; Castellano, F. N.; Chen, L. X., Coherence in Metal-Metal-to-Ligand-Charge-Transfer Excited States of a Dimetallic Complex Investigated by Ultrafast Transient Absorption Anisotropy. *J. Phys. Chem. A* **2011,** *115*, 3990–3996.

11. Kvapilová, H.; Sattler, W.; Sattler, A.; Sazanovich, I. V.; Clark, I. P.; Towrie, M.; Gray, H. B.; Záliš, S.; Vlček, A., Electronic Excited States of Tungsten(0) Arylisocyanides. *Inorg. Chem.* **2015,** *54*, 8518–8528.

12. Záliš, S.; Hunter, B. M.; Gray, H. B.; Vlček, A., Electronic Structures of Reduced and Superreduced $Ir_2(1,8$-diisocyanomenthane)$_4^{n+}$ Complexes. *Inorg. Chem.* **2017,** *56*, 2874–2883.

13. Hill, M. G.; Sykes, A. G.; Mann, K. R., Spectroelectrochemical Characterization of $Ir_2(dimen)^{4+}$ and $Ir_2(dimen)_4^{0}$ (dimen = 1,8-Diisocyanomenthane). *Inorg. Chem.* **1993,** *32*, 783–784.

14. Hunter, B. M.; Villahermosa, R. M.; Exstrom, C. L.; Hill, M. G.; Mann, K. R.; Gray, H. B., M−M Bond-Stretching Energy Landscapes for $M_2(dimen)_4^{2+}$ (M = Rh, Ir; dimen = 1,8-Diisocyanomenthane) Complexes. *Inorg. Chem.* **2012,** *51*, 6898–6905.

15. Exstrom, C. L.; Britton, D.; Mann, K. R.; Hill, M. G.; Miskowski, V. M.; Schaefer, W. P.; Gray, H. B.; Lamanna, W. M., Structures of $[M_2(dimen)_4](Y)_2$ (M = Rh, Ir; dimen = 1,8-Diisocyanomenthane; Y = PF_6, Tetrakis[3,5-bis(trifluoromethyl)phenyl]borate, $B(C_6H_5)_4$) Crystals Featuring an Exceptionally Wide Range of Metal-Metal Distances and Dihedral Twist Angles. *Inorg. Chem.* **1996,** *35*, 549-550.

16. Dohn, A. O.; Jónsson, E. O.; Kjær, K. S.; van Driel, T. B.; Nielsen, M. M.; Jacobsen, K. W.; Henriksen, N. E.; Møller, K. B., Direct Dynamics Studies of a Binuclear Metal Complex in Solution: The Interplay Between Vibrational Relaxation, Coherence, and Solvent Effects. *J. Phys. Chem. Lett.* **2014,** *5*, 2414–2418.

17. Liard, D. J.; Busby, M.; Matousek, P.; Towrie, M.; Vlček, A., Jr., Picosecond Relaxation of [3]MLCT Excited States of $[Re(Etpy)(CO)_3(dmb)]^{+}$ and $[Re(Cl)(CO)_3(bpy)]$ as Revealed by Time-Resolved Resonance Raman, IR and UV-Vis Absorption Spectroscopy. *J. Phys. Chem. A* **2004,** *108*, 2363-2369.

18. Blanco-Rodríguez, A. M.; Busby, M.; Ronayne, K. L.; Towrie, M.; Grădinaru, C.; Sudhamsu, J.; Sýkora, J.; Hof, M.; Záliš, S.; Di Bilio, A. J.; Crane, B. R.; Gray, H. B.; Vlček, A., Jr., Relaxation Dynamics of $[Re^I(CO)_3(phen)(HisX)]^{+}$ (X = 83, 107, 109, 124, 126) *Pseudomonas aeruginosa* Azurins. *J. Am. Chem. Soc.* **2009,** *131*, 11788-11800.

19. Turner, J. J., Bandwidths. In *Handbook of Vibrational Spectroscopy*, Chalmers, J.; Griffiths, P. R., Eds. Wiley: Chicherster, 2002; Vol. 1, pp 101-127.

20. Turner, J. J., Infrared vibrational band shapes in excited states. *Coord. Chem. Rev.* **2002,** *230*, 213-224.

21. Fischer, S. F.; Laubereau, A., Dephasing Processes of Molecular Vibrations in Liquids. *Chem. Phys. Lett.* **1975,** *35*, 6-12.

22. Wood, K. A.; Strauss, H. L., Broadening and Shifts of Vibrational Bands Due to the Effect of Thermal Chemical Reactions. *J. Phys. Chem.* **1990,** *94*, 5677-5684.

23. Tokmakoff, A.; Zimdars, D.; Urdahl, R. S.; Francis, R. S.; Kwok, A. S.; Fayer, M. D., Infrared Vibrational Photon Echo Experiments in Liquids and Glasses. *J. Phys. Chem.* **1995,** *99*, 13310-13320.

24. Tokmakoff, A.; Urdahl, R. S.; Zimdars, D.; Francis, R. S.; Kwok, A. S.; Fayer, M. D., Vibrational spectral diffusion and population dynamics in a glass-forming liquid: Variable bandwidth picosecond infrared spectroscopy. *J. Chem. Phys.* **1995,** *102*, 3919-3931.

25. Durrell, A. C.; Keller, G. E.; Lam, Y.-C.; Sýkora, J.; Vlček, A., Jr.; Gray, H. B., Structural Control of $^1A_{2u}$-to-$^3A_{2u}$ Intersystem Crossing in Diplatinum(II,II) Complexes. *J. Am. Chem. Soc.* **2012,** *134*, 14201–14207.

26. Záliš, S.; Lam, Y. C.; Gray, H. B.; Vlček, A., Jr., Spin−Orbit TDDFT Electronic Structure of Diplatinum(II,II) Complexes. *Inorg. Chem.* **2015,** *54*, 3491–3500.

27. Hofbeck, T.; Lam, Y. C.; Kalbáč, M.; Záliš, S.; Vlček, A.; Yersin, H., Thermally Tunable Dual Emission of the d^8-d^8 Dimer [Pt$_2$(μ-P$_2$O$_5$(BF$_2$)$_2$)$_4$]$^{4-}$. *Inorg. Chem.* **2016,** *55*, 2441–2449.

28. Lam, Y. C.; Gray, H. B.; Winkler, J. R., Intersystem Crossing in Diplatinum Complexes. *J. Phys. Chem. A* **2016,** *120*, 7671−7676.

29. Miskowski, V. M.; Rice, S. F.; Gray, H. B., Excited-State Decay Processes of Binuclear Rhodium(I) Isocyanide Complexes. *J. Phys. Chem.* **1993,** *97*, 4277-4283.

30. Miskowski, V. M.; Rice, S. F.; Gray, H. B.; Dallinger, R. F.; Milder, S. J.; Hill, M. G.; Exstrom, C. L.; Mann, K. R., Spectroscopy and Photophysics of Rh$_2$(dimen)$_4$$^{2+}$ (dimen = 1,8-Diisocyanomenthane). Exceptional Metal-Metal Bond Shortening in the Lowest Electronic Excited States. *Inorg. Chem.* **1994,** *33*, 2799-2807.

31. Cheng, S. C.; Blaine, C. A.; Hill, M. G.; Mann, K. R., Electrochemical and IR Spectroelectrochemical Studies of the Electrocatalytic Reduction of Carbon Dioxide by [Ir$_2$(dimen)$_4$]$^{2+}$ (dimen = 1,8-Diisocyanomenthane). *Inorg. Chem.* **1996,** *35*, 7704-7708.

32. Greetham, G. M.; Donaldson, P. M.; Nation, C.; Sazanovich, I. V.; Clark, I. P.; Shaw, D. J.; Parker, A. W.; Towrie, M., A 100 kHz Time-Resolved Multiple-Probe Femtosecond to Second Infrared Absorption Spectrometer. *Applied Spectroscopy* **2016,** *70*, 645–653.

For Table of Contents Only

$\nu(C\equiv N)$ IR signal

2101 cm^{-1}

Δ Absorbance

2215 cm^{-1}

2203 cm^{-1}

Time / ps